JOURNAL OF IRON AND STEEL RESEARCH, INTERNATIONAL. 2011, 18(9): 33-40

Influence of Carbon Content on Strain Hardening Behaviour of Sintered Plain Carbon Steel Preforms

S Narayan, A Rajeshkannan
(Mechanical Engineering, The University of the South Pacific, Laucala Campus, Suva 1168, Fiji)

Abstract: Complete experimental investigation on the instantaneous strain hardening behaviour of powder metallurgy (P/M) preforms of pure iron, Fe-0.35%C, Fe-0.75%C and Fe-1.1%C was carried out. The strain hardening behaviour of the above-mentioned P/M sintered steel preforms with aspect ratio of 0.4 under triaxial stress state condition was determined by cold upsetting under nil/no and graphite lubricant conditions. The instantaneous strain hardening value (n_i), strength coefficient (K_i), and the stress as a function of strain and densification were obtained and analyzed. Furthermore, a relation was obtained from a semi-log plot of stress against relative density and analyzed to study the hardening behaviour owing to densification as stress was a function of induced strain as well as densification in the P/M materials.

Key words: strain hardening exponent; density hardening exponent; strength coefficient; densification; triaxial stress

The forming of sintered metal powder preforms is currently studied extensively and is receiving a great deal of global interest as a progressive and economical method of producing components from metal powders. Powder metallurgy (P/M) is a near net shape metal forming technique used to manufacture part to close tolerance[1-2]. Powder metallurgy components are widely used in sophisticated industrial applications while the worldwide popularity lies in the ability of powder metallurgy technique to produce complex shapes with exact or very close tolerance at a very high production rate at minimal costs[3-4]. Quite often, powder metallurgy technique is used for material systems that are difficult to machine and difficult or impossible to cast. Powder preform forging involves the fabrication of a preform by primary deformation processing technique, followed by the secondary pressing of the preform to its final shape with substantial densification. The vast application of ferrous powder metallurgy material in automotive[5] and aerospace industry provides reasons for researchers to analyze powder metallurgy materials behaviour under metal forming processes[6-7]. Hence, the endeavor of the present researchers is producing parts to near theoretical density; however, 100% dense component cannot be produced. The prediction of failure in powder preform forging is important from the viewpoint of die design and selection of preform geometry, since material properties may affect the final shape of a deformed workpiece and may cause defects such as cracks or folds[8-9].

In powder preform forging, a porous material would experience the usual strain or work hardening characteristics as well as geometrical work hardening[10]. However, the rate of increase in the stress value with respect to strain is greater than that would be observed in a pore free material of the same composition under identical testing conditions, as the continued reduction in the porosity level during upsetting increases the load bearing cross sectional area. This in turn increases the stress required for further deformation, resulting in matrix and geometric work hardening behaviour. Thus, the total strain or work hardening behaviour of porous preform is due to the combined effects of induced densification and induced strain during cold forging[11-13]. By interfering with dislocation movement, grain boundaries also contribute to the characteristic property of a metal to become stronger as it is deformed, and the property referred to as strain hardening. Strain hardening is of major importance in forming

Biography: S Narayan(1982—), Male, Master, Assistant Lectureship; **E-mail**: narayan_su@usp.ac.fj; **Received Date**: June 25, 2010

operations since it controls the amount of uniform plastic strain, the material can undergo during cold upsetting before crack appears at the free surface. R Narayanasamy et al[14] investigated the instantaneous strain hardening behavior of an aluminum-iron powder metallurgy composite with various percent of iron contents and for the various stress state conditions with two different aspect ratios. It is well known that both the strain hardening exponent and the strength coefficient are basic mechanical behaviour performance parameters of metallic materials. Therefore, strain hardening exponent is an important parameter reflecting a material' s hardening property and its determination is of great importance[15]. It has been found out[10,16] that initial geometry of the powder metallurgy preform has an effect on the strain hardening exponent and strength coefficient. Further studies[9,17-19] show that as the carbon content increases, the pore size becomes smaller, which affects the deformation and densification behavior.

Thus, the present investigation aims to establish the strain hardening behaviour of powder metallurgy preforms of pure iron, Fe-0.35%C, Fe-0.75%C and Fe-1.1%C experimentally with the influence of lubricant conditions namely nil/no and graphite lubricant and to establish the technical relationship that exists between the characteristics of instantaneous strain hardening exponent with respect to percent fractional theoretical density and true height strain. Furthermore, the technical relationship is established that exists between instantaneous strength coefficient with respect to percent fractional theoretical density and true height strain. Also stress-strain and stress-densification relationship was established for the four powder metallurgy preforms under nil/no and graphite lubricant conditions for initial aspect ratio of 0.4. It is well known that for P/M materials, stress is a function of induced strain and densification, hence, a relationship is obtained from a semi-log plot of stress against relative density and analyzed.

1 Experimental

1.1 Materials and characterization

Atomized iron powder of size less than or equal to 150 μm and graphite powder with size of 2—3 μm were used in the present investigation. Analysis indicated that the purity of iron was 99.7% and the rest were insoluble impurities. The characteristic of iron powder, Fe-0.35% C, Fe-0.75% C and Fe-1.1%C blends are shown in Table 1 and Table 2.

Table 1 Characterization of iron powder

No.	Property	Iron	Fe-0.35%C blend	Fe-0.75%C blend	Fe-1.1%C blend
1	Apparent density/(g · cm^{-3})	3.38	3.37	3.29	3.21
2	Flow rate per 50 g powder measured by Hall flow meter/s	26.3	28.1	25.3	24.8
3	Compressibility at (430±10) MPa/(g · cm^{-3})	6.46	6.26	6.41	6.35

Table 2 Sieve size analysis of iron powder

Sieve size/μm	150	>125	>100	>75	>63	>45	<45
Retained matter in sieve/%	10.60	24.54	15.46	19.90	11.10	8.40	10.00

1.2 Blending, compaction and sintering

A powder mixture corresponding to Fe-0% C, Fe-0.35%C, Fe-0.75%C and Fe-1.1%C was taken in a stainless steel pot with the powder mixed to porcelain balls (10—15 mm in diameter) with a ratio of 1 : 1 by mass percent. The mill was operated for 20 h to obtain a homogenous mixing. Green compacts of 28 mm in diameter and 12 mm in length were prepared. The powder blend was compacted on a 1.0 MN hydraulic press using a suitable die, a punch and a bottom insert in the pressure range of (430±10) MPa to obtain an initial theoretical density of 0.84%. To avoid oxidation during sintering and cooling, the entire surface of the compacts was indigenously formed ceramic coated. These ceramic coated compacts were heated in the electric muffle furnace with temperature of 1 200 ℃. At this temperature, the compacts were sintered for 90 min followed by furnace cooling.

1.3 Cold deformation

Sintered and furnace cooled preforms were machined to such a dimension so as to provide height-to-diameter ratio of 0.40. Each specimen was compressively deformed between a flat die-set in the incremental loading step of 0.05 MN using 1 MN capacity hydraulic press under friction conditions, which in-

cluded dry, unlubricated dies called nil/no lubricant condition and lubrication consisting of graphite paste (i. e. graphite with acetone) called graphite lubricant condition. The deformation process was stopped once a visible crack appeared at the free surface. Dimensional measurements such as deformed height, deformed diameters (including bulged and contact) were carried out after every step of deformation and the density measurements being carried out using the Archimedes principle. Experimental results were used to calculate the flow stress, true height strain, percentage theoretical density and instantaneous strength coefficient (C_i and K_i), instantaneous density hardening index (m_i) and instantaneous strain hardening exponent (n_i).

2 Theoretical Analysis

Using the measured upsetting parameters, the following mathematical expressions are used to determine other upsetting parameters (instantaneous strain hardening and strength coefficient) for triaxial stress state. The expression for true axial stress and strain for P/M materials are as follows:

$$\sigma_z = P/A_Q \tag{1}$$

$$\varepsilon_z = \ln(h_o/h_f) \tag{2}$$

and true hoop strain is

$$\varepsilon_\theta = \ln[(2D_b^2 + D_c^2)/3D_o^2] \tag{3}$$

where, σ_z is the axial stress; P is the axial load; A_Q is the initial contact surface area; ε_z is the true axial strain; ε_θ is the true hoop strain; h_o is the initial height of the preform; h_f is the forged height of the preform; D_b is the forged bulged diameter of the preform; D_c is the forged contact diameter of the preform; and D_o is the initial diameter of the preform.

According to R Narayansamy et al[14], the hoop stress (σ_θ) under triaxial stress state condition can be determined as given below:

$$\sigma_\theta = [(2\alpha + R^2)/(2 - R^2 + 2R^2\alpha)]\sigma_z \tag{4}$$

where, $\alpha = d\varepsilon_\theta/d\varepsilon_z$; $d\varepsilon_z$ is the plastic strain increment in the axial direction; $d\varepsilon_\theta$ is the plastic strain increment in the hoop direction; and R is the relative density.

The effective stress σ_{eff} and the effective strain ε_{eff} are determined by the following expressions in terms of cylindrical coordinates as explained elsewhere[20-21] under triaxial stress state for axisymmetric upset forging condition ($\sigma_r = \sigma_\theta$, where σ_r is the radial stress).

$$\sigma_{eff} = \{[\sigma_z^2 + 2\sigma_\theta^2 - R^2(\sigma_\theta^2 + 2\sigma_z\sigma_\theta)]/2R^2 - 1\}^{0.5} \tag{5}$$

$$\varepsilon_{eff} = \left\{\left[\frac{2}{3(2+R)}\right][(\varepsilon_z - \varepsilon_\theta)^2 + (\varepsilon_\theta - \varepsilon_z)^2] + \left[\frac{(\varepsilon_z + 2\varepsilon_\theta)^2}{3}\right](1 - R^2)\right\}^{0.5} \tag{6}$$

Eqn. (5) and Eqn. (6) are utilized to determine the strain hardening parameters as explained here. An attempt was made to use plastic flow (Ludwik) equation $\sigma = K\varepsilon^n$, with little modification for P/M preforms to determine the instantaneous strength and instantaneous strain hardening, where σ is the true effective stress; ε is the true effective strain; K is the strength coefficient and n is strain hardening exponent. The theoretical description is given as follows.

Assuming the consecutive effective load on the preform is specified as 1, 2, 3, ···, $(x-1)$, and x, the plastic flow equation can be written as:

$$\sigma_x = K\varepsilon_x^n \tag{7}$$

$$\sigma_{x-1} = K\varepsilon_{x-1}^n \tag{8}$$

Subtracting Eqn. (7) and Eqn. (8), the following expression can be obtained

$$\sigma_x - \sigma_{x-1} = K(\varepsilon_x^n - \varepsilon_{x-1}^n) \tag{9}$$

Eqn. (9) can be further deduced into

$$K_i = (\sigma_x - \sigma_{x-1})/(\varepsilon_x^n - \varepsilon_{x-1}^n) \tag{10}$$

Now, dividing Eqn. (7) by Eqn. (8), the following expression is obtained

$$\sigma_x/\sigma_{x-1} = \varepsilon_x^n/\varepsilon_{x-1}^n = (\varepsilon_x/\varepsilon_{x-1})^n \tag{11}$$

Taking natural logarithm on both sides of Eqn. (11), it follows,

$$\ln(\sigma_x/\sigma_{x-1}) = n\ln(\varepsilon_x/\varepsilon_{x-1}) \tag{12}$$

Eqn. (12) can be further simplified into

$$n_i = \frac{\ln(\sigma_x/\sigma_{x-1})}{\ln(\varepsilon_x/\varepsilon_{x-1})} \tag{13}$$

Eqn. (10) and Eqn. (13) can be utilized for determining the instantaneous strength coefficient and instantaneous strain hardening exponent from the experimental data corresponding to stress and strain.

Furthermore, from the semi-log plot of stress against relative density, the following linear relationship can be deduced as

$$\lg\sigma = mR + \lg C \tag{14}$$

where, m is the density hardening index; and C is the density strength coefficient. Eqn. (14) can be reduced to a general form as

$$\sigma = Ce^{mR} \tag{15}$$

Assuming the consecutive effective load on the preform is specified as 1, 2, 3, ···, $(i-1)$, and i, Eqn. (15) can be written as

$$\sigma_i = Ce^{mR_i} \tag{16}$$

$$\sigma_{i-1} = Ce^{mR_{i-1}} \tag{17}$$

Dividing Eqn. (16) by Eqn. (17) gives

$$\sigma_i/\sigma_{i-1} = (Ce^{mR_i})/(Ce^{mR_{i-1}}) \tag{18}$$

Taking natural logarithm on both sides of Eqn. (18), it follows,

$$\ln(\sigma_i/\sigma_{i-1}) = m(R_i - R_{i-1}) \tag{19}$$

Eqn. (19) can be further simplified into

$$m_i=\frac{\ln(\sigma_i/\sigma_{i-1})}{R_i-R_{i-1}} \tag{20}$$

Using Eqn. (20), m_i can be determined. Furthermore, subtracting Eqn. (16) from Eqn. (17), the following expression can be obtained:

$$\sigma_i-\sigma_{i-1}=C(e^{mR_i}-e^{mR_{i-1}}) \tag{21}$$

Eqn. (21) can be further rearranged as:

$$C_i=\frac{\sigma_i-\sigma_{i-1}}{e^{mR_i}-e^{mR_{i-1}}} \tag{22}$$

From Eqn. (22), C_i can be determined.

3 Results and Discussion

3.1 Stress-densification characteristics

Fig. 1 has been constructed between flow stress and percentage fractional theoretical density for various P/M steel preforms during cold deformation under the influence of carbon content with initial theoretical density of 84%. The characteristics of the curve are that the flow stress increases as the densification also increases. Due to the continual application of the applied stress, the pores present in the P/M material collapse and close, thereby enhancing the densification and increasing the strength of the P/M material. To further deform the P/M preforms requires additional load; hence, the applied load is increased as the deformation and density increases. It is observed (Fig. 1) that during cold upsetting, the rate of densification of the P/M preforms exhibits three distinct stages. From beginning to 0.87 of relative density, the densification rate is slower with a rapid increase in flow stress; however, the flow stress values are lower. This is because the initial application of load is not sufficient to collapse and close the pores and the internal compressive stress increases and enhances the mobility of particles. When relative density is between 0.87 and 0.93, the densification rate follows a linear trend with gradual increase in densification. The slope of the curve during the intermediate stage is lower compared to the initial stage owing to substantial enhancement in the lateral deformation during the intermediate stage which in turn increases the load bearing capacity thus increasing the applied stress. Finally, when the relative density is above 0.93, an increase in stress values is observed with little densification owing to the work hardening of the material. It is seen (Fig. 1) that from initial density up to 0.93 of relative density, the flow stress is the highest for Fe-1.1% C for any given densification, followed by Fe-0.75%C, Fe-0.35%C and the lowest for pure iron. The smaller carbon particles (2—3 μm) fill the bigger pores between iron particles, reducing the pore size in the P/M preform. Hence, as the amount of smaller particle size (carbon particles) increases, the pore size in the P/M preform becomes smaller and the flow stress required is higher due to higher load requirements for further plastic deformation. Furthermore, the rate of densification is higher in the case of pure iron in comparison with Fe-1.1%C. The densification behaviour of Fe-0.35%C and Fe-0.75%C P/M preform is between Fe-1.1%C and pure iron P/M preform. Thus, from Fig. 1, it can be concluded that when the carbon content is reduced, the densification rate can be substantially enhanced. This behaviour is true during the initial and intermediate stage; however, during the final stage, the flow stress values increase substantially for the pure iron followed by Fe-0.35%C, Fe-0.75%C and the lowest for Fe-1.1%C P/M preform under dry friction conditions. This indicates that pure iron preform is strain-hardened at a faster and higher rate in comparison with other preforms. This is due to the bigger pores present in the pure iron preform which collapse and close at a faster rate than the smaller pores present in iron-carbon alloy preforms.

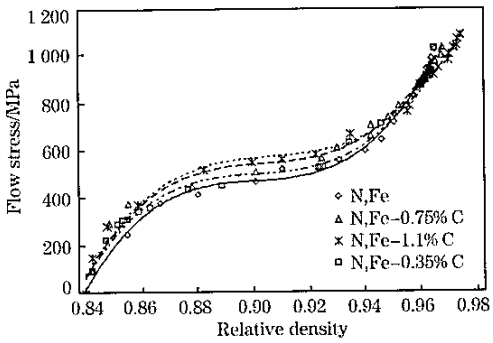

Aspect ratio of 0.4; N—Nil/no lubricant condition.

Fig. 1 Variation of flow stress with relative density for various P/M steels

Stress and strength of P/M materials depend on both strain and densification. As the P/M material is deformed, the pores in the P/M material collapse, enhancing the density and increasing the strength of the material, and in view of this, a semi-log plot is presented in Fig. 2 between stress in log scale against relative density. The relationship between true stress and relative density can be expressed as $\sigma=Ce^{(mR)}$, where C refers to density strength coefficient and m refers to density hardening exponent and these two parameters can be utilized to understand the stress

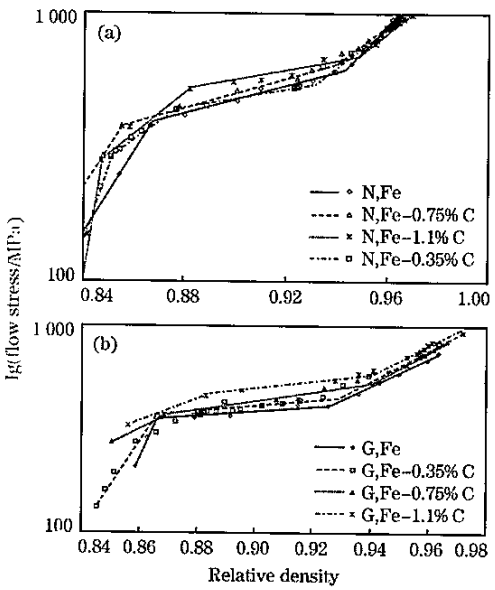

(a) Nil/no lubricant condition;
(b) Graphite lubricant condition.
Aspect ratio of 0.4; N—Nil/no lubricant condition; G—Graphite lubricant condition.

Fig. 2 Flow stress in log-scale for various P/M steels

densification phenomenon in enhancing the strength of the P/M material. The characteristics of the curves shown in Fig. 2 are similar and follow three different mechanisms. Table 3 shows the values for m_i and C_i obtained from Fig. 2 for different carbon contents and different frictional constraints and Fig. 3 is plotted to show the effect of carbon content in the P/M preform on density hardening exponent. Mechanism 1 can be neglected for all practical reasons as only few points are available for plotting (Fig. 2). Also initial application of stress is not sufficient to densify the preforms and during the initial stage, the material is able to resist the applied stress until it exceeded the initial yield stress; hence, mechanism 1 is neglected. From Table 3, it can be noted that as the mi values increase, the C_i values decrease for the same composition preform. Furthermore, it is seen that the m_i values are higher and the C_i values are lower in the case of nil/no lubricant condition in comparison with graphite lubricant condition. From Fig. 4, it can be seen that the m_i values decrease with increasing carbon content for nil/no lubricant; however, it is not the same result in the case

Table 3 Values of m_i and C_i of four steels

Composition	Mechanism of density hardening	Frictional constraints			
		Nil/no lubricant		Graphite lubricant	
		m_i	C_i	m_i	C_i
Fe	1	15.24	2.37×10^{-11}	28.16	1.86×10^{-22}
	2	2.55	2.38	0.99	59.10
	3	10.29	1.18×10^{-7}	5.35	5.48×10^{-3}
Fe-0.35%C	1	6.95	3.47×10^{-4}	17.94	1.40×10^{-13}
	2	1.78	11.91	1.14	45.45
	3	6.31	7.61×10^{-4}	6.4	5.81×10^{-3}
Fe-0.75%C	1	15.21	3.67×10^{-11}	5.62	5.85×10^{-3}
	2	2.67	2.00	1.95	8.86
	3	7.18	1.13×10^{-4}	6.36	6.13×10^{-4}
Fe-1.1%C	1	7.65	9.13×10^{-5}	4.26	9.19×10^{-2}
	2	1.30	36.75	1.64	18.89
	3	7.94	2.03×10^{-5}	5.46	4.78×10^{-3}

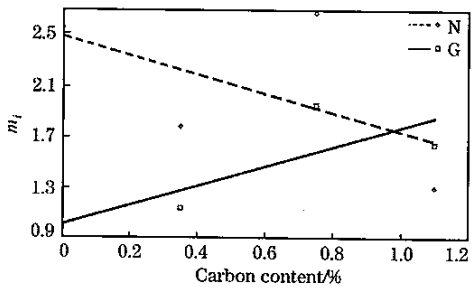

Fig. 3 Variation of density hardening exponent against carbon content

of graphite lubricant preform.

3.2 Stress-strain characteristics

Fig. 4 has been constructed between flow stress and true height strain for various P/M steel preforms during cold deformation under the influence of frictional constraints and carbon content with initial preform relative density of 84%. For any given true height strain, the flow stress increases with the increasing percentage of carbon content in the preform. The bigger pores are more prominent to collapse and

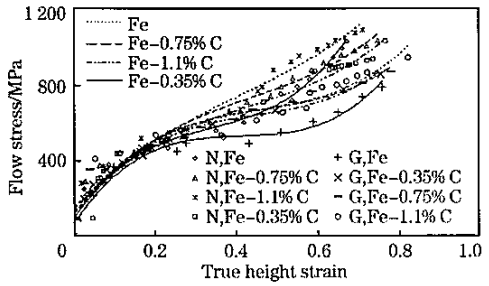

Aspect ratio of 0.4; N—Nil/no lubricant condition; G—Graphite lubricant condition.

Fig. 4 Variation of flow stress with true height strain for various P/M steels

close than smaller pores for P/M materials. As the carbon content increases, the pore size decreases, thereby enhancing the stress values. The behaviour is true irrespective of lubricants employed; however, the stress values are enhanced in the case of dry friction condition in comparison with graphite lubricant preform.

3.3 Strain hardening characteristics

It is well known that both the strain hardening exponent and the strength coefficient are basic mechanical behaviour performance parameters of metallic materials. Fig. 5 and Fig. 6 are drawn to show the relationship for n_i against relative density and axial strain, respectively, under the influence of carbon content and frictional constraints. The characteristics of the curves follow similar trend, a sudden increase in n_i values with little densification and deformation followed by a sudden decrease in the n_i values and then it follows a gradual increase for relative density of 0.86—0.95 and for axial strain of 0.05—0.55, respectively. For relative density above 0.95 and axial strain above 0.55, a mild to heavy fluctuations in n_i values are observed. This behaviour is true irrespective of lubricant employed. Initially, the applied stress is not sufficient to deform the large amount of pores and the stress values rise substantially for small amounts of densification and

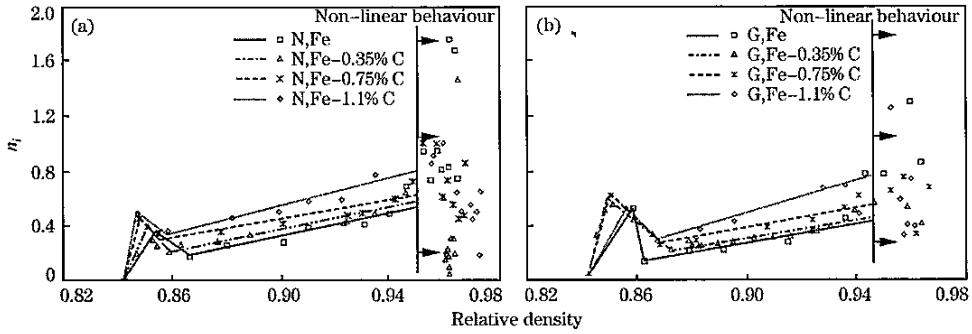

(a) Nil/no lubricant condition; (b) Graphite lubricant condition.

Fig. 5 Variation of instantaneous strain hardening exponent with relative density showing effect of carbon contents

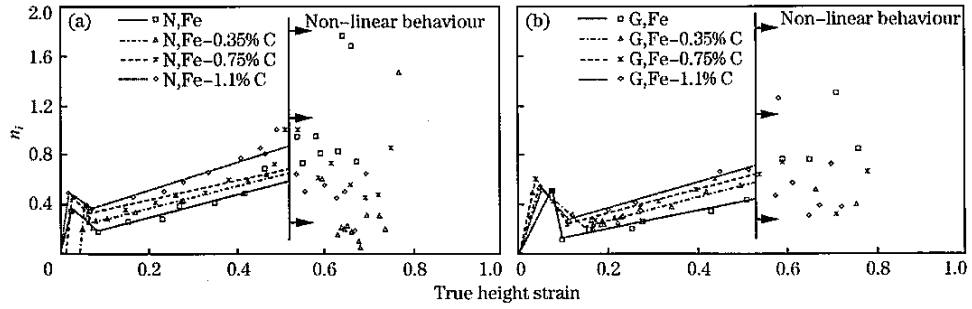

(a) Nil/no lubricant condition; (b) Graphite lubricant condition.

Fig. 6 Variation of instantaneous strain hardening exponent with true height strain showing effect of carbon contents

deformation (Fig. 1 and Fig. 4) is the reason for high n_i values initially which in no means increases the strength of material and can be neglected. During the final stage, the P/M material approaches near theoretical density with 4%—5% pores left, which are difficult to close. The preforms are highly strain hardened at this point; hence, to further close the remaining pores requires high applied stress, which

in turn significantly increases the n_i values and when these remaining pores collapse, the n_i values are significantly reduced. This causes fluctuations in the n_i values in the final stages of deformation. Furthermores, careful observations of Fig. 5 and Fig. 6 reveal that during the intermediate stage (relative density of 0.86—0.95 and axial strain of 0.05—0.55), the strain hardening is pronounced for Fe-1.1%C P/M steel and the n_i values decrease with the reducing carbon content in the preform. The increasing amount of carbon particles in the preform increases the number of smaller particles; therefore, more grains and grain boundaries are present. Hence, by interfering with dislocation movement, grain boundaries also contribute to the strain hardening of a P/M material to become stronger as it is deformed. Furthermore, from Fig. 5 and Fig. 6, it is noted that the n_i values are enhanced for nil/no lubrication in comparison with graphite lubrication and the fluctuations of n_i values are severe in the case of nil/no lubricant condition after relative density exceeds 0.95 or axial strain exceeds 0.55. It can be concluded that strain hardening is promoted in the P/M preform by increasing the amount of carbon content and increasing the frictional constraints.

Fig. 7 and Fig. 8 are drawn to show the relationship for K_i against relative density and axial strain, respectively, under the influence of carbon content and frictional constraints. The curves plotted in Fig. 7 and Fig. 8 show that the K_i increases rapidly at low values of densification and strain rate followed by a decrease in the K_i values. Thereafter, for relative density of 0.88—0.95 and axial strain of 0.17—0.55 respectively, the K_i increased at a steady state and for relative density above 0.95 and axial strain above 0.55, a fluctuation in the K_i values are noticed. The fluctuations in the K_i values are severe for nil/no lubrication in comparison with graphite lubricant employed. The slope of the curve during the intermediate stage is higher for nil/no lubricant condition compared to graphite lubricant employed; hence, increasing the frictional constraints enhances the strength coefficient. The plot of K_i against relative density shows that Fe-0.75%C under nil/no lubricant condition has enhanced strength coefficient values; however, in the case of graphite lubricant condition, Fe-1.1%C have shown enhanced strength coefficient values. The same phenomenon is observed

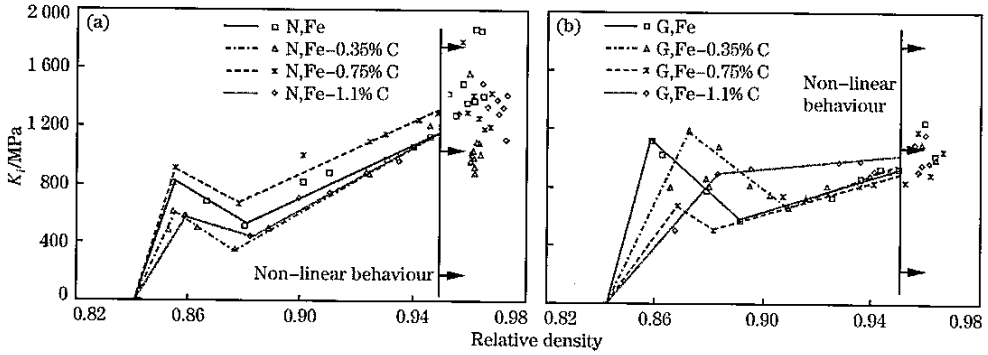

(a) Nil/no lubricant condition; (b) Graphite lubricant condition.

Fig. 7 Variation of instantaneous strength coefficient with relative density

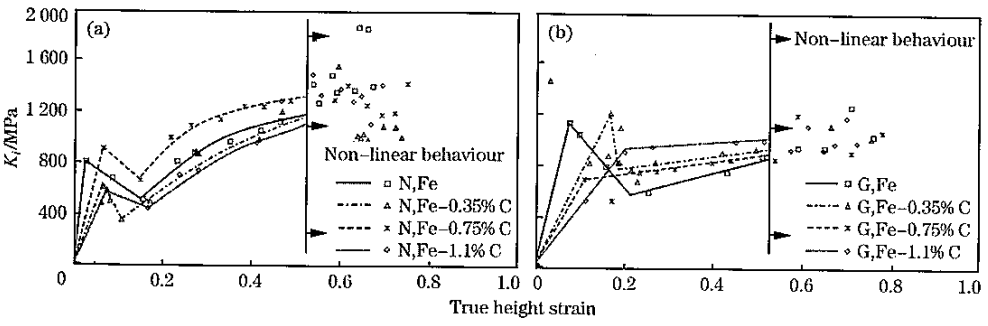

(a) Nil/no lubricant condition; (b) Graphite lubricant condition.

Fig. 8 Variation of instantaneous strength coefficient with true height strain under

for K_i plotted against a strain.

4 Conclusions

The densification rate is found to be low when increasing the carbon content in the P/M preform; however, the final density achieved is higher in the preform with highest carbon content. Furthermore, strain hardening exponent is improved with increasing carbon content in the P/M perform; however, the effect of carbon content on the strength coefficient is literally nil. Besides, strain hardening and strength coefficient in the P/M preform are improved when the frictional constraints are increased. Finally, two new parameters namely density hardening exponent and density strength coefficient are introduced to study hardening behaviour in P/M material by densification.

References:

[1] Agarwal M, Kumar S, Sutradhar G. Deformation of Solid Powder Discs and Strips Under Lubricated Condition [J]. J Mater Process Technol, 2002, 123(3): 440.

[2] Hua L, Qin X, Mao H, et al. Plastic Deformation and Yield Criterion for Compressible Sintered Powder Materials [J]. J Mater Process Technol, 2006, 180(1/2/3): 174.

[3] Kandavel T K, Chandramouli R, Ravichandran M. Experimental Study on the Plastic Deformation and Densification Characteristics of Some Sintered and Heat Treated Low Alloy Powder Metallurgy Steels [J]. Mater Des, 2010, 31(1): 485.

[4] Wang B, Zhang E. On the Compressive Behavior of Sintered Porous Coppers With Low-to-Medium Porosities—Part II: Preparation and Microstructure [J]. Int J Mech Sci, 2008, 50 (3): 550.

[5] Lindskog P. Economy in Car-Making—Powder Metallurgy [R]. London: Global Automotive Manufacturing and Technology, 2003.

[6] Narayanasamy R, Anandakrishnan V, Pandey K S. Effect of Carbon Content on Workability of Powder Metallurgy Steels [J]. Mater Sci Eng, 2008, 494A(1/2): 337.

[7] Narayanasamy R, Anandakrishnan V, Pandey K S. Effect of Molybdenum Addition on Workability of Powder Metallurgy Steels During Cold Upsetting [J]. Mater Sci Eng, 2009, 517A (1/2): 30.

[8] Rajeshkannan A, Narayan S. Strain Hardening Behaviour in Sintered Fe-0.8%C-1.0%Si-0.8%Cu Powder Metallurgy Preform During Cold Upsetting [J]. J Eng Manufacture, 2009, 223(12): 1567.

[9] Selvakumar N, Ganesan P, Radha P, et al. Modelling the Effect of Particle Size and Iron Content on Forming of Al-Fe Composite Preforms Using Neural Network [J]. Mater Des, 2007, 28(1): 119.

[10] Narayanasamy R, Pandey K S. Some Aspects of Work Hardening in Sintered Aluminium—Iron Composite Preforms During Cold Axial Forming [J]. J Mater Process Technol, 1998, 84(1/2/3): 136.

[11] Kahlow K J. Void Behaviour as Influenced by Pressure and Plastic Deformation [R]. Bethlehem: Institute for Metal Forming Report, Lehigh University, 1971.

[12] Taha M A, El-Mahallawy N A, El-Sabbagh A M. Some Experimental Data on Workability of Aluminium-Particulate-Reinforced Metal Matrix Composites [J]. J Mater Process Technol, 2008, 202(1/2/3): 380.

[13] Zhang X Q, Peng Y H, Ruan X Y, et al. Study of Workability Limits of Porous Materials Under Different Upsetting Conditions by Compressible Rigid Plastic Finite Element Method [J]. J Mater Eng Perform, 2000, 9(2): 164.

[14] Narayanasamy R, Ramesh T, Pandey K S. An Investigation on Instantaneous Strain Hardening Behaviour in Three Dimensions of Aluminium-Iron Composites During Cold Upsetting [J]. Mater Sci Eng, 2005, 391A(1/2): 149.

[15] Ebrahimi R, Pardis N. Determination of Strain-Hardening Exponent Using Double Compression Test [J]. Mater Sci Eng, 2009, 497A(1/2): 56.

[16] Pandey K S. Some Investigations on the Cold Deformation Behaviour of Sintered Aluminium-4% Copper Alloy Powder Preforms [J]. Int J Powder Met Sci Technol, 1991, 2(4): 45.

[17] Kandavel T K, Chandramouli R, Shanmugasundaram D. Experimental Study of the Plastic Deformation and Densification Behaviour of Some Sintered Low Alloy P/M Steels [J]. Mater Des, 2009, 30(5): 1768.

[18] DONG Xian-feng, HU Jian-dong, WANG Hong-ying, et al. A Study on Carbon Concentration Distribution and Microstructure of P/M Materials Prepared by Carbusintering [J]. J Mater Process Technol, 2009, 209(8): 3776.

[19] Fillabi M G, Simchi A, Kokabi A H. Effect of Iron Particle Size on the Diffusion Bonding of Fe-5%Cu Powder Compact to Wrought Carbon Steels [J]. Mater Des, 2008, 29(2): 411.

[20] Doraivelu S M, Gegel H L, Gunasekera J S, et al. A New Yield Function for Compressible P/M Materials [J]. Int J Mech Sci, 1984, 26(9/10): 527.

[21] Narayanasamy R, Anandakrishnan V, Pandey K S. Effect of Geometric Work-Hardening and Matrix Work-Hardening on Workability and Densification of Aluminium-3.5% Alumina Composite During Cold Upsetting [J]. Mater Des, 2008, 29 (8): 1582.